Commensurate States and Pattern Switching via Liquid Crystal Skyrmions Trapped in a Square Lattice

SCHOLARONE™
Manuscripts

ARTICLE TYPE

Commensurate States and Pattern Switching via Liquid Crystal Skyrmions Trapped in a Square Lattice

A. Duzgun[a], C. Nisoli[a], C. J. O. Reichhardt[*a], and C. Reichhardt[a]

Using continuum based simulations we show that a rich variety of skyrmion liquid crystal states can be realized in the presence of a periodic obstacle array. As a function of the number of skyrmions per obstacle we find hexagonal, square, dimer, trimer and quadrimer ordering, where the *n*-mer structures are a realization of a molecular crystal state of skyrmions. As a function of external field and obstacle radius we show that there are transitions between the different crystalline states as well as mixed and disordered structures. We discuss how these states are related to commensurate effects seen in other systems, such as vortices in type-II superconductors and colloids interacting with two dimensional substrates.

1 Introduction

Numerous hard and soft matter systems can be effectively modeled as an assembly of interacting particles coupled to a two dimensional (2D) periodic substrate. These include atoms and molecules on surfaces[1,2], vortices in type-II superconductors[3,4] or Bose-Eisenstein condensates[5,6] interacting with periodic pinning arrays, and charged[7–11] or magnetic colloids[12,13] on optical traps or structured surfaces. Such systems exhibit a variety of commensuration effects in the form of crystalline or superlattice states when the number of particles is an integer multiple of the number of substrate minima. One example is the colloidal molecular crystal states found in colloids on 2D arrays, where the colloids form localized clusters with synchronized orientational degrees of freedom[7–10]. In some cases plastic crystals[7,8] can form in which the number of particles per trap is fixed but there is no orientational ordering of the clusters.

Other particle-like objects are skyrmions, which arise when the collective behavior of underlying microscopic degrees of freedom leads to the formation of larger scale structures. For chiral magnetic systems, the underlying degrees of freedom are the spins[14–16], while for chiral liquid crystal systems, they are the molecular director orientations[17–20].

When a chiral liquid crystal is subjected to frustration by confinement or electric fields, twisted structures including confined blue phases[21], cholesteric bubbles[22,23], and cholesteric stripes also known as cholesteric fingers[23–26] can arise. In the case of very strong confinement or strong electric fields, a uniform nematic phase is favored as a result of the un-

winding of the chiral structures. Between the uniform nematic and cholesteric stripe phases, stable meron lattices, which are essentially a blue phase in which double twist cylinders form a hexagonal lattice, are both theoretically predicted and experimentally realized in the high chirality limit[21,27,28]. The blue phase can be controlled using a self-assembled substrate[29]. Baby skyrmions can also be stabilized between the cholesteric stripe and uniform nematic phases[18]. Unlike merons or half-skyrmions which are reported to exist only as lattices[28,30], skyrmions are observed as isolated local structures and are *local* objects that behave like soft particles. In contrast, merons are accompanied by defects or disclination lines. Due to these properties, skyrmions are ideal candidates for particle-like structures that can be controlled individually[31].

There has been growing interest in skyrmions and merons in liquid crystals due to the identification of new methods to create and control such systems[18,27,30,32–34]. There is also work examining how liquid crystal (LC) skyrmions can be manipulated externally[35], made to interact with barriers or pinning sites[36–38], or caused to form isolated or collective moving states[37,39].

Since LC skyrmions, which can be regarded as individual particles, can also be arranged to form lattices and interact with repulsive barriers, it is interesting to examine what types of LC skyrmion states could be realized when the LC is coupled a periodic substrate, and compare this behavior to the types of ordering found in other systems of particles coupled to ordered substrates. Duzgun and Nisoli[40] recently proposed that LC skyrmions interacting repulsively within a square or triangular array of obstacles can exhibit frustration effects similar to those found in artificial spin ice systems[41,42]. In this work we extend these ideas to examine the types of non-frustrated commensurate LC skyrmion lattices that can arise

[a] Theoretical Division and Center for Nonlinear Studies, Los Alamos National Laboratory, Los Alamos, New Mexico 87545, USA. Fax: 1 505 606 0917; Tel: 1 505 665 1134; E-mail: cjrx@lanl.gov

when the skyrmions are coupled to a square lattice of obstacles of the type that could be created by patterned external fields or surface anchoring[37,38,40]. We find that a rich variety of crystalline states can be stabilized, including a square lattice at a one to one matching, a dimer lattice for two skyrmions per obstacle, and staggered trimer and quadrimer orderings at three and four to one matching. These *n*-mer states are similar to the colloidal molecular crystal states observed on periodic substrates[7–10]; however, the skyrmions exhibit shape distortions that do not occur in the colloidal system.

We show that different structures can be accessed for fixed skyrmion number when the size of the obstacles is changed or the external field is varied. For the case of one to one matching, we observe a transition from a square to triangular lattice along with intermediate states in which the skyrmions form a mixed structure due to their ability to adopt different sizes in a single sample. There can also be pattern switching between different states when the size of all or a portion of the radii of the obstacles is varied or when an external field is changed, suggesting that LC skyrmions on patterned substrates could exhibit rapid large scale structural transitions that could be useful for applications.

2 Numerical Methods

We model an assembly of N LC skyrmions interacting with a square array of N_{obs} obstacles using continuum based simulations[20,40]. We consider the traceless tensor Q related to the scalar order parameter S that quantifies the orientational order of the chiral nematic liquid crystal state, which gives rise to solutions that support skyrmions when the chiral liquid crystal host is confined between two substrates with normal surface anchoring. The free energy density has the form

$$
\begin{aligned}
f = &(a/2)Tr(Q^2) + (b/3)Tr(Q^3) + (c/4)[(Tr(Q^2)]^2 \\
&+ (L/2)(\partial_\gamma Q_{\alpha\beta})(\partial_\gamma Q_{\alpha\beta}) - (4\pi/p)L\varepsilon_{\alpha\beta\gamma}Q_{\alpha\rho}\partial_\gamma Q_{\beta\rho} \\
&- [K(\delta(z) + \delta(z - N_z)) + E^2\Delta\varepsilon]Q_{zz}
\end{aligned}
$$

(1)

The first three terms above control the nematic to isotropic transition, the next two terms describe the elastic energies with respect to a gradient in Q, favoring a twist with cholesteric pitch p. Here we use a single elastic constant approximation following the description of Hornreich and Shtrikman[21]. The last term is due to the homeotropic surface anchoring at the boundaries and the external electric field, where K is the coupling strength, E is the electric field in the z-direction, and $\Delta\varepsilon$ is the dielectric anisotropy. On the confining surfaces, the Q tensor is coupled to a uniaxial perfect ordering in the z direction denoted by $Q_s = \begin{pmatrix} -1/2 & 0 & 0 \\ 0 & -1/2 & 0 \\ 0 & 0 & 1 \end{pmatrix}$. The electric field E

generated by applying a potential difference across the slab is assumed to be constant and pointing in the z direction everywhere inside the slab neglecting the variations caused by the anisotropy of the dielectric constants.

The states are evolved by simulating the following overdamped equation:

$$
\frac{\partial Q(r,t)}{\partial t} = -\Gamma \frac{\delta F}{\delta Q(r,t)},
$$

(2)

where Γ is the mobility constant and $F = \int f(x,y,z)\,dx\,dy\,dz$. We denote the field alignment strength as $\alpha = E^2\Delta\varepsilon$. A z-invariant structure can be achieved when vertical alignment of molecules is produced solely by the background electric field (*i.e.*, by choosing a very small $K \approx 0$ and appropriate value of α)[31,43]. Recently, experimental realizations of structures with weak z dependence have been achieved[44]. In the experiments, 2D skyrmions appear at around $N_z \approx p$, and when $N_z > p$, they become less stable. Since the experiments use surface anchoring, both the size and the shape of the skyrmions are sensitive to the cell thickness, whereas in our model, the background field maintains the stability of the skyrmions, the skyrmion shape is z invariant, and the skyrmion size is sensitive to the background field. For $K \approx 0$, a z invariant structure appears regardless of the cell thickness, though in practice, there may be some limitations on this invariance. The cell thickness is limited from below by how small a value of K can be generated on the confining substrate. While there is no theoretical upper limit on the thickness, experimental realizations are usually performed within up to a few cholesteric pitch lengths. In any event, the thickness must remain much smaller than the size of the parallel plates in order to avoid fringe effects which cause variations in the background field strength in both the radial and z directions. In this work we consider such a z-invariant case and model the system as a 3D director ($Q-$tensor) configuration lying on a 2D surface.

As in other work[20,40], we use obstacles that are produced by strongly aligning the directors along the z-axis. These obstacles are repulsive barriers of radius r which are realized by applying an additional electric field within the barrier region that is much stronger than the background field. The same effect can be achieved by means of strong surface anchoring localized within the barriers, which enters the free energy equation identically. We use the electric field because it permits dynamic control of the barrier size, shape, and strength. (See the discussion section for arguments regarding field.) We first let the system relax, swell the skyrmion size, and then bring the skyrmions to a fixed size, which allows for a dynamical annealing effect. Experimentally this would be achieved varying the external field. Since we discuss the effect of electric field on skyrmion size in great detail in a previous work[20], here we merely note that reducing the background electric field causes the skyrmions to swell, and increasing it causes them to shrink.
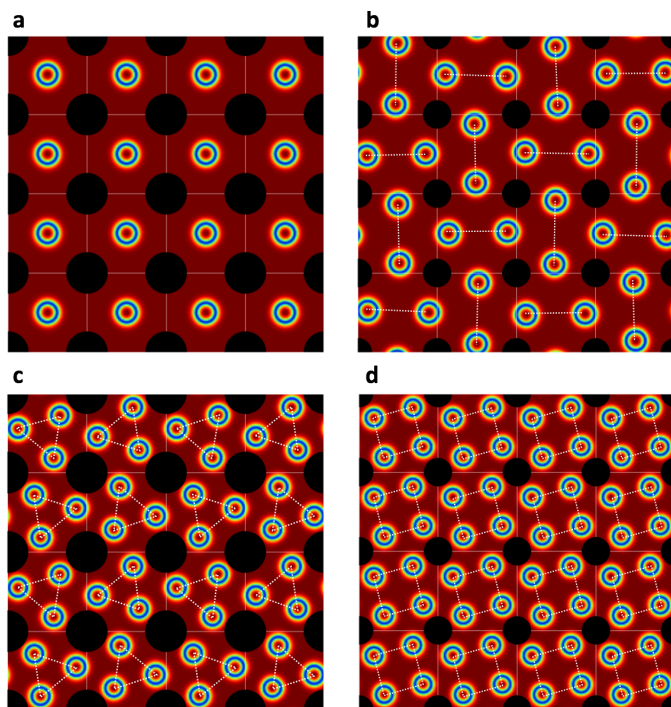
Fig. 1 The liquid crystal skyrmions (blue rings) and obstacle locations (black circles) obtained from a continuum based simulation of a chiral liquid crystal state. In each case $\alpha = 0.3$. The colors represent the orientation of the director field. (a) The 1:1 matching at an obstacle radius of $r = 15$ showing a square skyrmion lattice. (b) The 2:1 state at $r = 10$ with an alternating dimer ordering as indicated by the white dashed lines. (c) The 3:1 state at $r = 15$ where there is trimer ordering with a small shift at every other plaquette. (d) The 4:1 state showing a quadrimer ordering at $r = 10$. Here the size of the square cells is $L = 60$.

After the relaxation, we reduce the background field to swell the skyrmions instead of modifying the strong extra field that produces the barriers. For the periodic obstacle array we find that a single swell cycle is adequate; however, for more complex geometries or a random array, a repeated swell cycle can be applied. We focus on a system size of 4×4 barriers for filling ratios of skyrmions to obstacles of 1 : 1 up to 4 : 1. For specific cases we have also considered larger arrays of up to 20×20 which show the same ground states[45].

3 Results

In Fig. 1(a) we show the location of the barriers of spacing $L = 60$ and the skyrmions at $r = 15$. Here there is a 1:1 matching of the number of skyrmions to the number of obstacles. The skyrmions form a square lattice located in the center of the interstitial regions between the obstacles. Figure 1(b) shows the case of two skyrmions per obstacle with

$r = 10$, where the system forms a dimer lattice as indicated by the dashed lines connecting pairs of skyrmions. The dimers have an additional long range orientational ordering, and each dimer is alternately vertical or horizontal. In Fig. 1(c), at the 3 : 1 matching with $r = 15$, the skyrmions form an ordered trimer state as indicated by the lines. The trimers exhibit an additional small canting from one plaquette to the next. At 4 : 1 with $r = 10$ in Fig. 1(d), the skyrmions form a quadrimer state which is the same for each plaquette. These states are similar to the N-mer orderings found in colloidal molecular crystal systems for colloids interacting with square or triangular substrates[7–10]. In particular, the dimer state has been described as an anti-ferromagnetic Ising model on a square lattice[9], where the orientation of the dimer corresponds to the two possible orientations of an effective spin. A similar dimer state was also predicted for vortices in a Bose-Einstein condensate on a square lattice at the second matching filling[5]. The trimer ordering in the colloidal system[7] differs from that for the skyrmions in Fig. 1(c). The colloidal trimers have stripe or columnar orientational ordering due to the longer range multipolar charge interaction between trimers, whereas the LC skyrmion trimers experience only short range repulsion and have only weak orientational ordering along the horizontal direction. The LC skyrmion state has the same ordering as the colloidal state at the fourth filling for the square lattice[7]. We call the states in Fig. 1(b,c,d) LC skyrmion molecular crystals since the N-mers have both positional and orientational order.
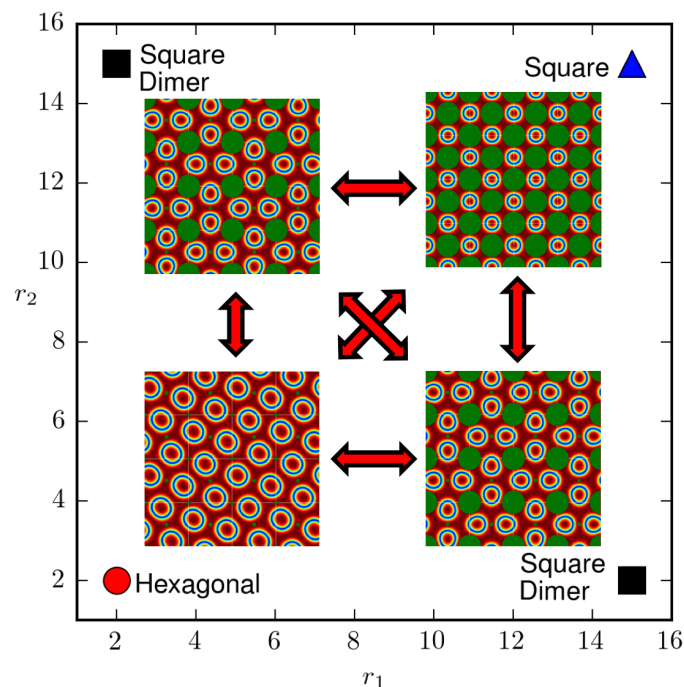
We next consider the effect of changing the background field and also the obstacle radius for the 1 : 1 filling. We change the background field to control the size of the skyrmions and we change the *extra field* inside the barriers to control the barrier size. For vortices and other particle based systems on a square array at the first matching filling, there can be a transition from a square lattice at strong coupling where the substrate dominates the behavior to a triangular lattice at weak coupling where the particle-particle interaction dominates the behavior[46,47]. For hard disks at a 1 : 1 matching on a square lattice, there can be a transition to a hexagonal lattice and even a rhombic phase as a function of substrate strength and disk size[48]. In Fig. 2(a) we show the phase diagram as a function of the obstacle radius r versus background field α for the 1 : 1 filling, where we observe five phases. For large fields $\alpha > 0.35$, skyrmions do not appear and the system has a uniform background. For large defect radius $r > 5.0$, there is an extended region in which the system forms a commensurate square lattice, as illustrated in Fig. 2(b). The square lattice extends over the range $6.0 < r < 16.0$, but we focus on the regime $r < 7.0$ since this is where additional phases occur. When r is small but α is large, the skyrmions have more room to distort, allowing them to form a hexagonal lattice as shown in Fig. 2(c). There is a window at $r = 3$ where, for small α, the skyrmions can more easily change shape to cre-
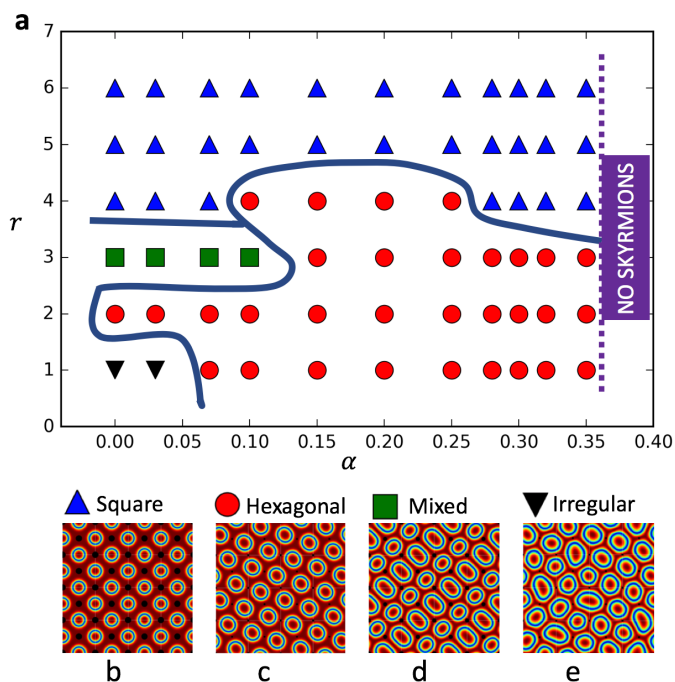
Fig. 2 (a) The phase diagram as a function of obstacle size r vs the background field α for the system in Fig. 1(a) at a 1:1 matching of LC skyrmions to obstacles. Blue triangles: square lattice states, shown in panel (b); red squares: hexagonal lattices, shown in panel (c); green squares: mixed state, shown in panel (d); black triangles: disordered or irregular states, shown in panel (e). For fields greater than $\alpha = 0.35$, skyrmions do not form, while for $6.0 < r < 16.0$ there is only a square lattice state.

Fig. 3 The different possible states for LC skyrmions on a square lattice at a 1:1 filling where the obstacles have two different radii, r_1 and r_2. When r_1 and r_2 are both large, the system forms a square lattice (upper left). When r_1 and r_2 are both small, hexagonal ordering emerges (lower right). For $r_1 \gg r_2$ or $r_2 \gg r_1$ (lower left and upper right), a dimer lattice emerges. The arrows indicate the different routes that could be taken to get from one state to another.

ate a mixed state as illustrated in Fig. 2(d). In this case, half of the skyrmions become elongated and the overall pattern has a superlattice ordering. At small obstacle radius and small field we find a disordered state with skyrmions in a mixture of sizes, as shown in Fig. 2(e). For other fillings, a similar phase diagram can be constructed, where obstacles of large size produce N-mer states, while disordered or hexagonal lattices generally form for smaller r. The transitions shown on the phase diagram are continuous due to the deformability of the skyrmions.

The fact that different patterns can arise as a function of obstacle size suggests that various types of pattern switching could be achieved by suddenly changing the sizes of all or a portion of the obstacles. An example of how this could be achieved for fixed skyrmion number is shown in Fig. 3, where half of the obstacles have radius r_1 and the other half have radius r_2. Here the background field is fixed at $\alpha = 0.2$. When r_1 and r_2 are both large, the system forms a square lattice as shown in the upper right panel. If r_1 and r_2 are both small, a hexagonal lattice appears as illustrated in the lower left panel, while for the cases of r_1 much smaller than r_2 or r_2 much

smaller than r_1, the system forms the dimer lattice indicated in the upper left and lower right corners. The arrows indicate the possible routes along which the different patterns could be switched. This suggests that LC skyrmions interacting with ordered structures can undergo large scale switching behaviors that could be useful for creating devices.

In Fig. 4 we plot the ratio of the distance between skyrmions, as indicated in the rectangular box in the inset, of side a and side b versus r_2/r_1 for the system in Fig. 3, where we fix $r_1 = 15$ and vary r_2. We show results for external field values of $\alpha = 0.16$ to $\alpha = 0.32$. When $a/b = 1.0$, we find a square lattice, while for $a/b = 0.5$, a dimer lattice appears. Upon increasing α, the transition to the square lattice shifts to higher ratios of r_2/r_1; however, at $\alpha = 0.32$ the system remains in the square lattice for all values of r_1/r_2 since the skyrmions are so small that they no longer interact with one another and show little distortion from their initial positions. This indicates that not only can the skyrmion pattern be switched, but also the geometric ratio of the pattern can be controlled as function of the electric field.
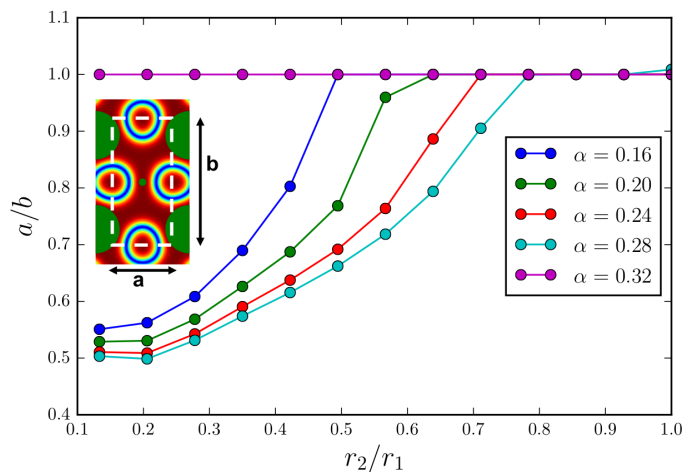
Fig. 4 The ratio of the sides a/b (shown in the inset) vs r_2/r_1 for samples from Fig. 3 with $1:1$ matching at $r_1 = 15$. When $a/b = 1.0$, the system forms a square lattice, while for $a/b \approx 0.5$, an ordered dimer lattice appears. For varied α or changing obstacle size, transitions occur between the two states.

4   Discussion

Our results should be general for even higher fillings N, leading to higher order N-mer states. For finite thermal fluctuations, the different states could show additional effects such as a transition from a molecular crystal state to a plastic crystal state in which the N-mers are randomly rotating, similar to what has been observed in colloidal molecular crystal systems[7–10]. Beyond commensurate states, there should also be a number of incommensurate states at non-integer matchings, which could form partially disordered states or rational commensurate states when the ratio of skyrmions to obstacles is rational. In particle based systems, incommensurate states form kinks or antikinks[49–51]. In the LC skyrmion system, however, due to the ability of the skyrmions to change size, the kinks can shrink or expand in order to reduce the energy cost of the defect, so that LC skyrmions could be much more robust to disordering due to incommensurations. Additionally, the irregular phase found at low background fields could exhibit glassy behavior. These results could also be extended to other obstacle lattice geometries such as triangular lattices, mixed lattices, quasiperiodic lattices, or random arrays.

In commensurate-incommensurate systems, a variety of dynamics can arise[49,50] when the system is driven. Driving of LC systems has already been demonstrated[39], so the dynamics of the skyrmions could be explored for driving over a periodic substrate. Finally, similar states could arise for magnetic skyrmions coupled to a periodic obstacle array, and there are already proposals on how to create such substrates for magnetic skyrmions on an anti-dot lattice[52]. Similarities between

the Hamiltonian for the liquid crystal skyrmions and that for magnetic skyrmions have already been noted[19,39].

Our model for the barriers is simple but sufficient: we produce the barriers by applying a strong extra field perpendicular to the plane of the LC cell. The field is uniform inside the barrier and zero outside. In real physical systems, such sharp gradients do not exist, but we use this approximation for thin samples to impose the effect of a barrier; in the SI we include results showing smooth gradients of the field. For the dynamic switching of the lattice structure, we allow the size of the barriers to be variable. This model can be modified in order to reflect possible experimental challenges. For instance, varying the barrier size does not imply that it is necessary to change the size of the electrodes; it can be achieved by varying the field. The size of the barrier does not need to be changed slowly, since the purpose of reducing the barrier size is to switch to a different packing ratio of skyrmions. The extra field producing the barrier can be turned off abruptly as well. We note that there will be fringe effects, since the field will be maximum at the center of the barrier and decay along the radius. Therefore, when the potential difference is reduced or even turned off, the effective radius of the barriers will continuously drop instead of changing instantaneously. We also propose that very small electrodes can be used so that the fringe effect is amplified and the field actually goes to zero at a certain distance from the center. In a separate work[31], we demonstrate that the electric field from point electrodes successfully produce repulsive regions with controllable size that drive skyrmions, and we show that if point electrodes are placed at distances $\pm H$ from the middle of the parallel plates, the field vanishes within a radius $\leq 2H$. In the supplementary material, we include a single layer simulation of dynamic switching in which the barriers are produced by point electrodes ($\alpha = \alpha_0 \exp(-5r^2/r_0^2)$) and the effective size is controlled by varying the strength of the electric field.

5   Summary

We have used continuum based simulations to examine the ordering of liquid crystal skyrmions interacting with a square obstacle array which could be created using anchoring or with fields. As a function of filling, we find that a variety of crystalline states can be stabilized, including a square lattice, an alternating dimer lattice, a trimer state, and a quadrimer state. We refer to the dimer and higher order N-mer states as skyrmion LC molecular crystal states in analogy to colloidal molecular crystals. For the commensurate $1:1$ filling, we map out the phase diagram as a function of barrier size and field and show that five different phases arise: no skyrmions, a square lattice, a hexagonal lattice, a disordered state, and a mixed phase. The mixed phase consists of a superlattice of skyrmions of different sizes. We also show that the system

can exhibit pattern switching between dimer, hexagonal and square lattices as a function of the ratios of the sizes of alternating obstacles. This can be generalized to programmed switching of obstacles in any pattern. We discuss future directions such as incommensurate states, other obstacle lattice geometries, and driving. Liquid crystal skyrmions represent another system that can be used to realize commensurate states for an assembly of particle-like objects coupled to a periodic substrate.

6 Acknowledgements

References

1 S. N. Coppersmith, D. S. Fisher, B. I. Halperin, P. A. Lee and W. F. Brinkman, *Phys. Rev. B*, 1982, **25**, 349–363.

2 P. Bak, *Rep. Prog. Phys.*, 1982, **45**, 587–629.

3 K. Harada, O. Kamimura, H. Kasai, T. Matsuda, A. Tonomura and V. V. Moshchalkov, *Science*, 1996, **274**, 1167–1170.

4 C. Reichhardt and N. Grønbech-Jensen, *Phys. Rev. Lett.*, 2000, **85**, 2372–2375.

5 H. Pu, L. O. Baksmaty, S. Yi and N. P. Bigelow, *Phys. Rev. Lett.*, 2005, **94**, 190401.

6 S. Tung, V. Schweikhard and E. A. Cornell, *Phys. Rev. Lett.*, 2006, **97**, 240402.

7 C. Reichhardt and C. J. Olson, *Phys. Rev. Lett.*, 2002, **88**, 248301.

8 M. Brunner and C. Bechinger, *Phys. Rev. Lett.*, 2002, **88**, 248302.

9 R. Agra, F. van Wijland and E. Trizac, *Phys. Rev. Lett.*, 2004, **93**, 018304.

10 A. Šarlah, T. Franosch and E. Frey, *Phys. Rev. Lett.*, 2005, **95**, 088302.

11 T. Brazda, A. Silva, N. Manini, A. Vanossi, R. Guerra, E. Tosatti and C. Bechinger, *Phys. Rev. X*, 2018, **8**, 011050.

12 P. Tierno, *Phys. Rev. Lett.*, 2016, **116**, 038303.

13 A. Libál, D. Y. Lee, A. Ortiz-Ambriz, C. Reichhardt, C. J. O. Reichhardt, P. Tierno and C. Nisoli, *Nature Commun.*, 2018, **9**, 4146.

14 S. Mühlbauer, B. Binz, F. Jonietz, C. Pfleiderer, A. Rosch, A. Neubauer, R. Georgii and P. Böni, *Science*, 2009, **323**, 915–919.

15 X. Z. Yu, Y. Onose, N. Kanazawa, J. H. Park, J. H. Han, Y. Matsui, N. Nagaosa and Y. Tokura, *Nature (London)*, 2010, **465**, 901–904.

16 N. Nagaosa and Y. Tokura, *Nature Nanotechnol.*, 2013, **8**, 899–911.

17 A. N. Bogdanov, U. K. Rößler and A. A. Shestakov, *Phys. Rev. E*, 2003, **67**, 016602.

18 P. J. Ackerman, R. P. Trivedi, B. Senyuk, J. van de Lagemaat and I. I. Smalyukh, *Phys. Rev. E*, 2014, **90**, 012505.

19 A. O. Leonov, I. E. Dragunov, U. K. Rößler and A. N. Bogdanov, *Phys. Rev. E*, 2014, **90**, 042502.

20 A. Duzgun, J. V. Selinger and A. Saxena, *Phys. Rev. E*, 2018, **97**, 062706.

21 R. M. Hornreich and S. Shtrikman, *Phys. Rev. A*, 1990, **41**, 1978–1989.

22 T. Akahane and T. Tako, *Japan. J. Appl. Phys.*, 1976, **15**, 1559–1560.

23 Y. Guo, S. Afghah, J. Xiang, O. D. Lavrentovich, R. L. B. Selinger and Q.-H. Wei, *Soft Matter*, 2016, **12**, 6312–6320.

24 P. Oswald, J. Baudry and S. Pirkl, *Phys. Rep.*, 2000, **337**, 67 – 96.

25 I. I. Smalyukh, B. I. Senyuk, P. Palffy-Muhoray, O. D. Lavrentovich, H. Huang, E. C. Gartland, V. H. Bodnar, T. Kosa and B. Taheri, *Phys. Rev. E*, 2005, **72**, 061707.

26 G. Durey, H. R. O. Sohn, P. J. Ackerman, E. Brasselet, I. I. Smalyukh and T. Lopez-Leon, *Soft Matter*, 2020, c9sm02033k.

27 J. Fukuda and S. Žumer, *Nature Commun.*, 2011, **2**, 246.

28 A. Nych, J. Fukuda, U. Ognysta, S. Žumer and I. Musevic, *Nature Phys.*, 2017, **13**, 1215 –1220.

29 J. Yang, J. Liu, B. Guan, W. He, Z. Yang, J. Wang, T. Ikeda and L. Jiang, *J. Mater. Chem. C*, 2019, **7**, 9460.

30 S. Wang, M. Ravnik and S. Žumer, *Liquid Crystals*, 2018, **45**, 2329–2340.

31 A. Duzgun, A. Saxena and J. V. Selinger, arXiv:2001.09615.

32 L. Cattaneo, v. Kos, M. Savoini, P. Kouwer, A. Rowan, M. Ravnik, I. Muševič and T. Rasing, *Soft Matter*, 2016, **12**, 853–858.

33 A. Nych, J. Fukuda, U. Ognysta, S. Žumer and I. Muševič, *Nature Phys.*, 2017, **13**, 1215.

34 D. Foster, C. Kind, P. J. Ackerman, J.-S. B. Tai, M. R. Dennis and I. I. Smalyukh, *Nature Phys.*, 2019, **15**, 655.

35 H. R. O. Sohn, C. D. Liu, Y. Wang and I. I. Smalyukh, *Optics Express*, 2019, **27**, 29055–29068.

36 P. J. Ackerman, Z. Qi and I. I. Smalyukh, *Phys. Rev. E*, 2012, **86**, 021703.

37 H. R. O. Sohn, C. D. Liu and I. I. Smalyukh, *Nature Commun.*, 2019, **10**, 4744.

38 H. R. O. Sohn, C. D. Liu, R. Voinescu, Z. Chen and I. I. Smalyukh, arXiv:1911.04640.

39 P. J. Ackerman, T. Boyle and I. I. Smalyukh, *Nature Commun.*, 2017, **8**, 673.

40 A. Duzgun and C. Nisoli, arXiv:1908.03246.

41 C. Nisoli, R. Moessner and P. Schiffer, *Rev. Mod. Phys.*, 2013, **85**, 1473–1490.

42 A. Ortiz-Ambriz, C. Nisoli, C. Reichhardt, C. J. O. Reichhardt and P. Tierno, arXiv:1909.13534.

43 G. De Matteis, L. Martina and V. Turco, *Theor. Math. Phys.*, 2018, **196**, 1150–1163.

44 J.-S. B. Tai and I. I. Smalyukh, arXiv:1911.07829.

45 See supplementary information for the larger system sizes.

46 C. Reichhardt, C. J. Olson, R. T. Scalettar and G. T. Zimányi, *Phys. Rev. B*, 2001, **64**, 144509.

47 B. Gränz, S. E. Korshunov, V. B. Geshkenbein and G. Blatter, *Phys. Rev. B*, 2016, **94**, 054110.

48 T. Neuhaus, M. Marechal, M. Schmiedeberg and H. Löwen, *Phys. Rev. Lett.*, 2013, **110**, 118301.

49 T. Bohlein, J. Mikhael and C. Bechinger, *Nature Mater.*, 2012, **11**, 126–130.

50 A. Vanossi, N. Manini and E. Tosatti, *Proc. Natl. Acad. Sci. (USA)*, 2012, **109**, 16429–16433.

51 D. McDermott, J. Amelang, L. M. Lopatina, C. J. O. Reichhardt and C. Reichhardt, *Soft Matter*, 2013, **9**, 4607–4613.

52 J. Feilhauer, S. Saha, J. Tobik, M. Zelent, L. J. Heyderman and M. Mruczkiewicz, arXiv:1910.07388.